Physics of Fluids

A lattice Boltzmann study of rarefied gaseous flow with convective heat transfer in backward facing micro-step

Cite as: Phys. Fluids **32**, 062005 (2020); https://doi.org/10.1063/5.0008325
Submitted: 21 March 2020 . Accepted: 29 May 2020 . Published Online: 19 June 2020

Ehsan Kamali Ahangar, Soroush Fallah-Kharmiani, Shabnam Dolati Khakhian, and Lian-Ping Wang (王连平)

Physics of Fluids ARTICLE scitation.org/journal/phf

A lattice Boltzmann study of rarefied gaseous flow with convective heat transfer in backward facing micro-step

Cite as: Phys. Fluids 32, 062005 (2020); doi: 10.1063/5.0008325
Submitted: 21 March 2020 • Accepted: 29 May 2020 •
Published Online: 19 June 2020

Ehsan Kamali Ahangar,[1,a)] Soroush Fallah-Kharmiani,[1] Shabnam Dolati Khakhian,[2] and Lian-Ping Wang (王连平)[3,4]

AFFILIATIONS

[1]Department of Mechanical Engineering, Ferdowsi University of Mashhad, Mashhad 91775-1111, Iran
[2]Department of Biomedical Engineering, Amirkabir University of Technology, Tehran 15916-34311, Iran
[3]126 Spencer Laboratory, Department of Mechanical Engineering, University of Delaware, Newark, Delaware 19716-3140, USA
[4]Department of Mechanics and Aerospace Engineering, Southern University of Science and Technology, Shenzhen, Guangdong 518055, China

[a)]**Author to whom correspondence should be addressed:** ehsan.kamali@mail.um.ac.ir

ABSTRACT

Rarefied pressure-driven gaseous flow with heat transfer in a microchannel with a backward facing micro-step is investigated in this paper using the lattice Boltzmann method (LBM) in slip and transition flow regimes. In a novel approach, a two-relaxation-time LB equation is used to solve the flow velocity and the single-relaxation-time to handle the heat transfer. The asymmetric relaxation time is determined by equating the analytical second-order slip velocity boundary condition and the slip velocity obtained from applying the implemented bounce back specular boundary condition in the LBM. A second-order implicit temperature jump boundary condition is also implemented to capture the rarefaction effect on the fluid temperature at walls. Velocity slip, temperature jump, centerline temperature, and Nusselt number variations are evaluated for channels with and without the micro-step for a wide range of the Knudsen number. Effects of the micro-step on the rarefied gaseous flow and convective heat transfer are evaluated and discussed. The numerical model is verified by comparing with direct simulation Mont Carlo results.

NOMENCLATURE

A	molecular slip coefficient
BSR	bounce back-specular reflection
c	Lattice speed ($\frac{lu}{tu}$)
C^*	temperature jump coefficient
$\boldsymbol{c}_i$	discrete velocity vectors ($\frac{lu}{tu}$)
c_s	speed of sound ($\frac{lu}{tu}$)
$DSMC$	direct simulation Monte Carlo
f	local distribution function (for fluid flow)
g	local distribution function (for heat transfer)
H	height of the microchannel (lu)
H_{in}	height of the microchannel inlet (lu)
h_s	height of the micro-step (lu)
Kn	Knudsen number, $Kn = \lambda/H$
L	length of the microchannel (lu)
L_s	length of the micro-step (lu)
LBM	Lattice Boltzmann method
Ma	Mach number
Nu	Nusselt number
P	pressure ($\frac{mu}{lu.(tu)^2}$)
Pr	Prandtl number
R	gas constant ($\frac{(lu)^2}{Tu.(tu)^2}$)
r	spatial position (lu)
Re	Reynolds number
S	bounce back fraction in BSR boundary condition

SRT	single relaxation time
T	temperature (Tu)
T^{jump}	temperature jump (Tu)
T_{mean}	bulk temperature (Tu)
t	time (tu)
TRT	two relaxation times
U^*	non-dimensional velocity
U_{mean}	mean velocity ($\frac{lu}{tu}$)
$\boldsymbol{V}$	velocity vector ($\frac{lu}{tu}$)
x	location (lu)

Greek symbols

α	thermal diffusivity ($\frac{(lu)^2}{tu}$)
δt	time step (tu)
δx	step by step (lu)
λ	molecular mean free path (lu)
Π	pressure ratio
ρ	density ($\frac{mu}{(lu)^3}$)
σ	TMAC coefficient
τ_a	anti-symmetric relaxation time (based on slip boundary)
τ_s	symmetric relaxation time (based on viscosity)
γ	heat capacity ratio
ω_i	weight factors

Subscript/Superscript

a	anti-symmetric
eq	equilibrium
i	discrete lattice directions
in	inlet
out	outlet
s	symmetric
w	wall

where (lu), (tu), (mu), and (Tu) stand for lattice unit, time unit, mass unit, and temperature unit in the LBM, respectively.

I. INTRODUCTION

Rapid development of the microelectromechanical systems (MEMS) in the last two decades and their applications in medical, aerospace, and mechanics sciences along with other small scale applications, such as extraction of the shale gas, drive the need for experimental and numerical studies on the rarefied gaseous flow and heat transfer at micro- and nano-scales. The gas flow at high altitudes and micro- and sub-micro-scales is the rarefied one, and the Knudsen number determines the rate of the rarefaction.[1]

Experimental studies are usually challenging and expensive due to the small dimension of microdevices. Therefore, numerical analysis of fluid flow and heat transfer at micro- and nano-scales becomes a viable alternative. For simulating such flows, the direct simulation Mont Carlo (DSMC),[2,3] lattice Boltzmann method (LBM),[4] and discrete velocity method (DVM)[5,6] are more accurate and effective than the continuum based methods because the Navier–Stokes (N–S) equations are not valid in the transition regime, and molecular interactions are not explicitly considered therein. The LBM takes advantage of much lower computational time compared to the DSMC, making the method a good and robust alternative to DSMC. In the following, representative studies based on DSMC, N–S solvers, and LBM for simulating the rarefied flow and heat transfer are reviewed.

Taassob *et al.*[7] simulated rarefied gaseous flow in a curved microchannel using the DSMC method. They found that increasing radius of the corner leads to a higher mass flow rate, and using a curvature instead of a sharp bend leads to an increased average shear stress and velocity slip.

Gavasane *et al.*[8] simulated the rarefied gaseous flow and heat transfer in a channel with backward facing micro-step using the DSMC. They reported that the mass flow rate is reduced with the rarefaction and flow separation is alleviated with the Knudsen number as well. Guerrieri *et al.*[9] investigated rarefied non-isothermal gaseous flow in diverging microchannels using the DSMC. They reported that the divergent channel increases the mass flow rate and thus the thrust in microresistojets. Hadj-Nacer *et al.*[10] also simulated rarefied gaseous flow between two co-axial cylinders and planar planes using the continuum based and DSMC methods in the slip regime.

Biswas *et al.*[11] simulated flow in a channel with a step for a wide range of Reynolds numbers and different expansion ratios in both 2D and 3D. The finite-volume method was employed for their simulations. They found that the length of the wake region is increased nonlinearly with the expansion ratio. Titarev[12] investigated a rarefied gaseous flow in a planar microchannel using the Boltzmann kinetic equation with the linearized S-model collision integral. He used a finer mesh near the walls and evaluated mass and heat transfer rates for the length-to-width ratio up to 1000 and a wide range of Kn numbers in both pressure-driven and thermal creep flows. He found that there is a recirculation region in the thermal creep flow, which is not observed in the pressure-driven one.

Ho *et al.*[13] investigated penetration of rarefied gas in a porous media in 2D using LBM with the multiple relaxation time (MRT) collision model. Circular and squared domains were studied and the Darcy formulation was used for calculating the penetration. They studied effects of the rarefaction, geometry of the porous media, and the porosity on the penetration rate. They reported that the penetration rate is increased with the rarefaction and is independent of the geometry. Wang *et al.*[14] also simulated the rarefied gaseous flow in the porous media using the MRT LBM. They evaluated the velocity field, the porosity effect, and the penetration rate. They reported that the penetration rate is considerably influenced by the pressure and is increased with the increase in porosity.

Meng and Zhang[5] studied the accuracy of the higher-order LB model in capturing non-equilibrium distribution function (NEDF) effects in rarefied gaseous flow both analytically and numerically. They reported that in the incompressible limit, the LB equation is reduced to the linear Bhatnagar-Gross-Krook (BGK) equation; therefore, LBM becomes very similar to the discrete velocity model (DVM) when the Gauss–Hermite approximation is used. Moreover, the order of the Hermite expansion for the NEDF has no direct relation with the Knudsen number for the incompressible flow in the BGK equation. Their numerical results show that using the higher-order terms in the NEDF leads to better capture of the non-equilibrium effects in the low velocity flows and increases the precision of results. They also reported that using the Gauss–Hermite approximation, the DVM and LBM lead to the similar results.

Ansumali *et al.*[15] showed that using a higher order LB equation improves the capability of the method for simulating the rarefied flows. Kim *et al.*[16] reported that this modification captures the rarefaction effects for the slip regime, but it is not reliable for the transition one as the simulated mass flow rate can become inaccurate.

Yang *et al.*[17] performed a comprehensive parametric investigation of the discrete velocity method and higher Lattice Boltzmann method (HLBM) for the rarefied gaseous flows. They reported a significant difference between the DVM and HLBM. They indicated that the HLBM is more efficient for low Knudsen numbers, while the DVM has better performance for high Knudsen numbers.

Ahangar *et al.*[18] simulated an isothermal rarefied gaseous flow in a microchannel with a backward micro-step using the two-relaxation-time (TRT) LBM in both slip and transition regimes. The TRT model reduces the computational cost and modeling difficulty compared to the MRT LBM. They evaluated effects of the *Kn* number and the micro-step on the velocity field and wake formation, local Mach number, and pressure variation.

Kharmiani and Roohi[19] simulated transitional gaseous flow in divergent micro/nanochannels for a wide range of the divergence angle, *Kn* number, and pressure ratio using the TRT LBM. They reported that there is a critical divergence angle at which the Knudsen (or Mach) number remains constant along the channel. This angle is linearly dependent on the pressure ratio only. Ahangar *et al.*[20] simulated rarefied gaseous flow in a microchannel with variable cross section using the TRT LBM for a wide range of *Kn* numbers. Ambrus and Sofonea[21] introduced a LB model based on the Gauss–Hermite squared summation method. They compared velocity, temperature, and heat flux results of the 2D Couette flow from LB models based on the Gauss–Hermite squared summation and Laguerre methods. They reported that the Hermite model is superior for $Kn > 0.05$.

In terms of thermal studies, Hadjiconstantinou and Simek[22] studied heat transfer in micro/nanochannels with a constant wall temperature using the DSMC method. They found that the Nusselt number is decreased with the increase in the Knudsen number. Renksizbulut *et al.*[23] simulated the rarefied gaseous slip flow and heat transfer in a microchannel using the finite volume method, solving the N–S and energy equations. They observed a sharp decrease in the friction factor and the Nusselt number in the entrance region of the microchannel due to the rarefaction effects. Rovenskaya[24] investigated the rarefied gaseous flow and heat transfer in a right-angle microchannel in three dimensions in slip regime, solving the compressible N–S and energy equations coupled with the first order slip velocity model and Smoluchowski temperature jump. He evaluated effects of the rarefaction and compressibility. He also found that the secondary flow produces an extra pressure drop and the secondary flow is weakened rapidly due to the dominant viscosity effects.

Niu *et al.*[25] used a thermal lattice Boltzmann model for microthermal flows. They found that the Nusselt number and local friction coefficient are reduced with an increase in the *Kn* number through a microchannel. They also investigated effects of the 3D microchannel aspect ratios (*AR*). Tian *et al.*[26] studied the Couette flow with heat transfer in the slip flow regime with the Maxwell first-order slip velocity model and the temperature jump by using lattice Boltzmann method. In terms of LBM, there are considerable works reported in the literature due to the inherent advantages of the method, such as the computational efficiency and modeling simplicity.

Gokaltun and Dulikravich[27] made a thermal LBM investigation on the rarefied slip flow in a microchannel and studied effects of the *Kn* number on the velocity and temperature distribution. They reported that as the *Kn* number is increased, both temperature jump and flow temperature are increased, but the Nusselt and friction factor are decreased. Furthermore, the velocity and temperature of the wall are higher in the entrance region of the channel.

Previous LBM studies of the rarefied flow and heat transfer in a microchannel in the transition regime used both the MRT collision operator and TRT collision operator for solving the flow field. It appears that the TRT LBM yields results as accurate as the MRT LBM for simulating the rarefied flow;[18,19] therefore, the TRT LBM is a better choice due to computational efficiency and model simplicity.

In this paper, the TRT LB equation is used to solve the flow and the single-relaxation-time (SRT) LBM for heat transfer in a microchannel with a micro-step for the first time. The bounce back specular (BSR) boundary condition is used to capture the slippage velocity and a second-order implicit boundary condition is implemented to capture the temperature jump on the walls. Using this TRT-SRT LBM, the rarefied pressure-driven fluid flow and heat transfer are evaluated at different Knudsen numbers. The linear Boltzmann, Information Preservation (IP), and DSMC results are used to validate our proposed model.

II. NUMERICAL MODEL

A. Computational domain

Figure 1 depicts the considered microchannel with a backward micro-step and considered boundary conditions for our investigation of the rarefied gaseous flow and heat transfer in this paper. The flow is driven by applying a pressure difference along the streamwise direction x characterized by the pressure ratio $\Pi = \frac{P_{in}}{P_{out}} = 2$. A constant temperature T_{in} and zero temperature gradient are applied on the inlet and outlet, respectively. The wall temperature $T_w = 0(Tu) < T_{in} = 1(Tu)$ is applied on the channel walls. The channel aspect ratio (AR) equals $L/H = 20$. The step length and height are $L_s = L/3$ and $h_s = H/4$, respectively. The inlet height of the channel thus equals $H_{in} = \frac{3}{4}H$. The expansion ratio is defined as $ER = \frac{H}{H_{in}} = 1.33$. In the numerical simulation, all parameters are defined in lattice units of *lu*, *mu*, *Tu*, and *tu* for the length, mass, temperature, and time, respectively.

B. TRT LBM for the rarefied fluid flow

The TRT LB equation comprised of the symmetric and asymmetric parts is given by[18]

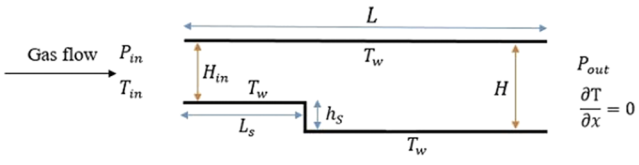

FIG. 1. A schematic of the considered problem.

$$f_i(r + \boldsymbol{c}_i\delta t, t + \delta t) = f_i(r,t) + \frac{\delta t}{\tau_s}\left[f_i^{eq}(r,t) - f_i(r,t)\right]_s + \frac{\delta t}{\tau_a}\left[f_i^{eq}(r,t) - f_i(r,t)\right]_a, \quad (1)$$

$$f_i^s = \frac{1}{2}(f_i + f_{-i}),\ f_i^a = \frac{1}{2}(f_i - f_{-i}), \quad (2)$$

where f is the particle distribution function (PDF), r is the spatial position, $\delta t = 1$ is the time step, $\boldsymbol{c}_i$ are the discrete velocity vectors of the considered D_2Q_9 lattice model, τ_s is the symmetric relaxation time, related to the fluid viscosity by $\nu = \frac{1}{3}(\tau_s - 0.5)$, and τ_a is the asymmetric relaxation time, related to the slip velocity model and sub/super scripts s and a indicate the symmetric and asymmetric values, respectively.

The equilibrium distribution function is as follows:[28]

$$f_i^{eq} = \omega_i\rho\left[1 + \frac{\boldsymbol{c}_i.\boldsymbol{V}}{{c_s}^2} + \frac{(\boldsymbol{c}_i.\boldsymbol{V})^2}{2{c_s}^4} - \frac{\boldsymbol{V}.\boldsymbol{V}}{2{c_s}^2}\right], \quad (3)$$

where the weight factors are given by[29]

$$\omega_i = \begin{cases} \frac{4}{9}, & i = 0 \\ \frac{1}{9}, & i = 1,2,3,4 \\ \frac{1}{36}, & i = 5,6,7,8. \end{cases} \quad (4)$$

The discrete particle velocity vectors are as follows:[18]

$$\boldsymbol{c_i} = c\begin{bmatrix} 0 & 1 & 0 & -1 & 0 & 1 & -1 & -1 & 1 \\ 0 & 0 & 1 & 0 & -1 & 1 & 1 & -1 & -1 \end{bmatrix}, \quad c = 1. \quad (5)$$

The speed of sound equals ${c_s}^2 = RT = \frac{c^2}{3} = \frac{1}{3}$ and the macroscopic flow variables are obtained from the PDF moments as follows:[20]

$$\rho = \sum_{i=0}^{8} f_i, \quad \boldsymbol{V} = \frac{1}{\rho}\sum_{i=0}^{8} f_i\boldsymbol{c}_i, \quad P = \rho{c_s}^2. \quad (6)$$

For modeling the rarefaction, the symmetric relaxation time is related to the Kn number as follows:[18]

$$\tau_{s(slip\ regime)} = \sqrt{\frac{6}{\pi}}\frac{H \cdot Kn}{\delta x} + \frac{1}{2}, \quad (7)$$

$$\tau_{s(Transitional\ regime)} = \sqrt{\frac{6}{\pi}}\frac{H \cdot Kn}{[1 + f(Kn)]\delta x} + \frac{1}{2}, \quad f(Kn) = \beta \cdot Kn, \quad (8)$$

where $\beta = 2$ according to the literature, which is adopted in this paper as well.

C. SRT LBM for the heat transfer

The general LB equation with single-relaxation-time for thermal rarefied gas flow is presented as follows:[30]

$$g_i(r + \boldsymbol{c}_i\delta t, t + \delta t) = g(r,t) + \frac{\delta t}{\tau_g}\left[g_i^{eq}(r,t) - g_i(r,t)\right], \quad (9)$$

$$g_i^{eq} = \omega_i T\left[1 + \frac{\boldsymbol{c}_i \cdot \boldsymbol{V}}{{c_s}^2}\right], \quad (10)$$

where τ_g is the thermal relaxation time, which is related to the thermal diffusivity as $\alpha = (\tau_g - 0.5){c_s}^2$. The macroscopic temperature is given by[30]

$$T = \sum_{i=0}^{8} g_i. \quad (11)$$

D. Boundary conditions

The pressure inlet and outlet are applied using the Zou–He boundary condition.[30] The BSR boundary condition is implemented in this paper for modeling and capturing the velocity slip of the gas at the walls. For example, for the lower wall of the channel, the BSR is applied as follows:[31]

$$\begin{bmatrix} f_5 \\ f_2 \\ f_6 \end{bmatrix} = \begin{bmatrix} s & 0 & 1-s \\ 0 & 1 & 0 \\ 1-s & 0 & s \end{bmatrix}\begin{bmatrix} f_7 \\ f_4 \\ f_8 \end{bmatrix}, \quad (12)$$

where s is a parameter between 0 and 1 such that $s = 0$ leads to the full no-lisp bounce-back and $s = 1$ leads to the full slip specular boundary condition. Therefore, varying the value of this parameter directly changes the slip velocity.

By equating the slip velocity equation obtained from applying the BSR boundary condition in LBM and the well-known analytical second order velocity slip equation, the asymmetric relaxation time and s are related to the coefficients of the second order model as follows:[18]

$$\tau_a = \frac{\pi A_2(2\tau_s - 1)^2 + 3}{8(2\tau_s - 1)} + 0.5, \quad s = 1\Big/\left(1 + \sqrt{\frac{\pi}{6}}A_1\right), \quad (13)$$

where A_1 and A_2 are the coefficient of Kn and Kn^2 term, respectively, in the second-order analytical slip velocity relation, $u_s = A_1\lambda\left.\frac{\partial u}{\partial y}\right|_{wall} - A_2\lambda^2\left.\frac{\partial^2 u}{\partial y^2}\right|_{wall}$. We set $A_1 = (1 - 0.1817\sigma)$ and $A_2 = 0.8$, where $\sigma = 1$ to model fully diffuse walls.[20] It should be clarified that for the slip flow regime, only the first order slip coefficient is considered and is sufficient for reasonably capturing the slip velocity. Based on the MD analysis conducted by Maxwell in 1879, $A_1 = 1$. Other research based on different analysis such as BGK kinetic model, Lattice Boltzmann equation (LBE), and theoretical analysis also obtained and reported values around 1. Based on the BGK kinetic model, Loyalka[32] reported the value of $A_1 = (1 - 0.1817\sigma)$, which is adopted in the current paper. However, subsequent research revealed that the first-order slip relation fails to predict the slip velocity as Kn is increased to the transition regime. Therefore, researchers added the second-order term to the relation as a correction. Since this correction had no clear Kinetic basis, various A_2 coefficients including $A_2 = 0.8$ proposed by Li *et al.*,[33] obtained from LBM, are reported in the literature corresponding to different analytical and numerical results.

For applying the constant temperature on the inlet, the method of non-equilibrium distribution functions is used.[27] The fully developed thermal condition, the zero temperature gradient, is imposed at the channel outlet.

The analytical temperature jump, at the upper wall, for example, is given by[27]

$$T_{y=H}^{jump} = T_w - T_{y=H} = \left(\frac{2\gamma}{\gamma + 1}\right)\left(\frac{Kn}{Pr}\right)\left(\frac{\partial T}{\partial y}\right)_{y=H}. \quad (14)$$

The fluid temperature at the wall therefore can be calculated from the equation with second order accuracy as follows:[27]

$$T_{y=H} = \frac{\left[C^*(4T_{jmax-1} - T_{jmax-2}) + 2T_w\right]}{(2+3C^*)}, \tag{15}$$

where $C^* = K \cdot Kn$ and $K = \left(\frac{2\gamma}{(\gamma+1)\cdot Pr}\right)$. Then, the unknown PDFs can simply be calculated as follows:[27]

$$g_4 = T_{y=H}(\omega(2) + \omega(4)) - g_2, \tag{16}$$

$$g_8 = T_{y=H}(\omega(6) + \omega(8)) - g_6, \tag{17}$$

$$g_7 = T_{y=H}(\omega(7) + \omega(5)) - g_5. \tag{18}$$

III. MODEL VERIFICATION AND VALIDATION

The mesh independency study in the present LBM is indicated in Table I. The micro-scale rarefied gas flow is simulated at Kn = 0.055 for four different mesh sizes of 200 × 10, 400 × 20, 800 × 40, and 1600 × 80. At this Kn number, the fluid velocity at the midpoint of the channel, $Y^* = \frac{Y}{H} = 0.5$, is selected for the four grid numbers. On the basis of calculated velocity values in Table I, the lowest error is between two mesh sizes 800 × 40 and 1600 × 80. Mesh size 800 × 40 is used for the numerical simulation due to less running time compared to the mesh size of 1600 × 80.

The DSMC, linear Boltzmann (analytical approach), and IP results are used to validate our numerical model for the fluid flow and heat transfer. For the former, an isothermal flow in a straight microchannel with constant cross section at AR = 20 and PR = 2 is considered. The non-dimensional velocity profile [relative to mean velocity (U_{mean}), $U^* = \frac{U}{U_{mean}}$] along the Y-direction ($Y^* = \frac{Y}{H}$) at Kn = 1.13 and the pressure deviation from the linear pressure $\delta P = \frac{[P(x)-P_l]}{P_{out}}$, where $P_L = P_{in} + \left(\frac{X}{L}\right)(P_{out} - P_{in})$,at two outlet Kn numbers (at $X^* = \frac{X}{L} = 1$), are compared with those of DSMC,[34] linear Boltzmann (Ohwada *et al.*),[35] and IP[36] methods in Figs 2(a) and 2(b), respectively, where a good agreement is observed. To validate the thermal part, two considered test conditions in the regular microchannel, without the step, are reported in Table II.

Figures 2(c) and 2(d) show variation of the non-dimensional centerline temperature, $T^* = \frac{T}{T_i}$, and the temperature jump along the channel at an inlet Knudsen number of 0.055, which are compared with corresponding DSMC results.[37] As observed, an excellent and fair agreement with DSMC is obtained for Case No. 1 and Case No. 2, respectively. For Case No. 2, the predicted temperature jump values by LBM and DSMC methods are 1.094 and 1.015, respectively. The calculated maximum error is roughly 7% occurred at the microchannel inlet. In Figs. 2(c) and 2(d), some discrepancies between the results of the present simulation and those of the DSMC are observed near the inlet and outlet, and the discrepancy increases with the wall temperature. This could be due to the stochastic errors associated with the finite temperature jump at the inlet when the inlet temperature and the wall temperature are different, as well as the difficulty of simulating the zero-gradient condition at the outlet in DSMC.

To evaluate the model for the fluid flow and heat transfer in the transition regime, simulation results are compared with those of DSMC results conducted by Gavasane *et al.*[8] at Kn_{in} = 1.3247. The test case parameters are provided in Table III. Figures 2(e)–(g) show the pressure, Ma, and temperature distribution, respectively, along the $Y^* = \frac{Y}{H} = 0.5$ and Fig. 2(h) shows the temperature jump at $Y^* = 1$ (top wall) in the microchannel with the backward facing micro-step. As observed in Figs. 2(e) and 2(f), there is an excellent agreement between two simulation results. The pressure and Ma number trends are vice versa, as expected. The centerline temperature and temperature jump distribution also show a good agreement with DSMC, with maximum discrepancy of 2.5% and 1%, respectively.

IV. RESULTS AND DISCUSSION

The considered parameters for numerical simulation in this section are as follows: 800 × 40 mesh domain, PR = 2, Pr = 0.7, $T_w = T_{bottom} = T_{top} = 0$ (Tu), and $T_{in} = 1$ (Tu). Furthermore, different Kn numbers mentioned in the following results are the inlet ones. The expansion ratio is set to ER = 1.33 unless otherwise mentioned. Figure 3 shows variations of the non-dimensional pressure, $P^* = P/P_{out}$, at $Y = H/2$ for the regular [Fig. 3(a)] and with micro-step [Fig. 3(b)] microchannels at three inlet Kn numbers. For the regular channel in Fig. 3(a), the fluid flow with a higher Knudsen number has a lower pressure value. As observed, the pressure reduces and tends from non-linear to the linear trend as the Kn number increases. In other words, there is a direct correlation between the Kn number and

TABLE I. Transverse velocities at different cross sections at a specific point.

Grid numbers			
(1) 200 × 10	(2) 400 × 20	(3) 800 × 40	(4) 1600 × 80
Velocity at $Y^* = \frac{Y}{H} = 0.5$			
1.238	1.310	1.349	1.367
Error (%)			
5.816 [Between (1) and (2)]		2.977 [Between (2) and (3)]	1.334 [Between (3) and (4)]

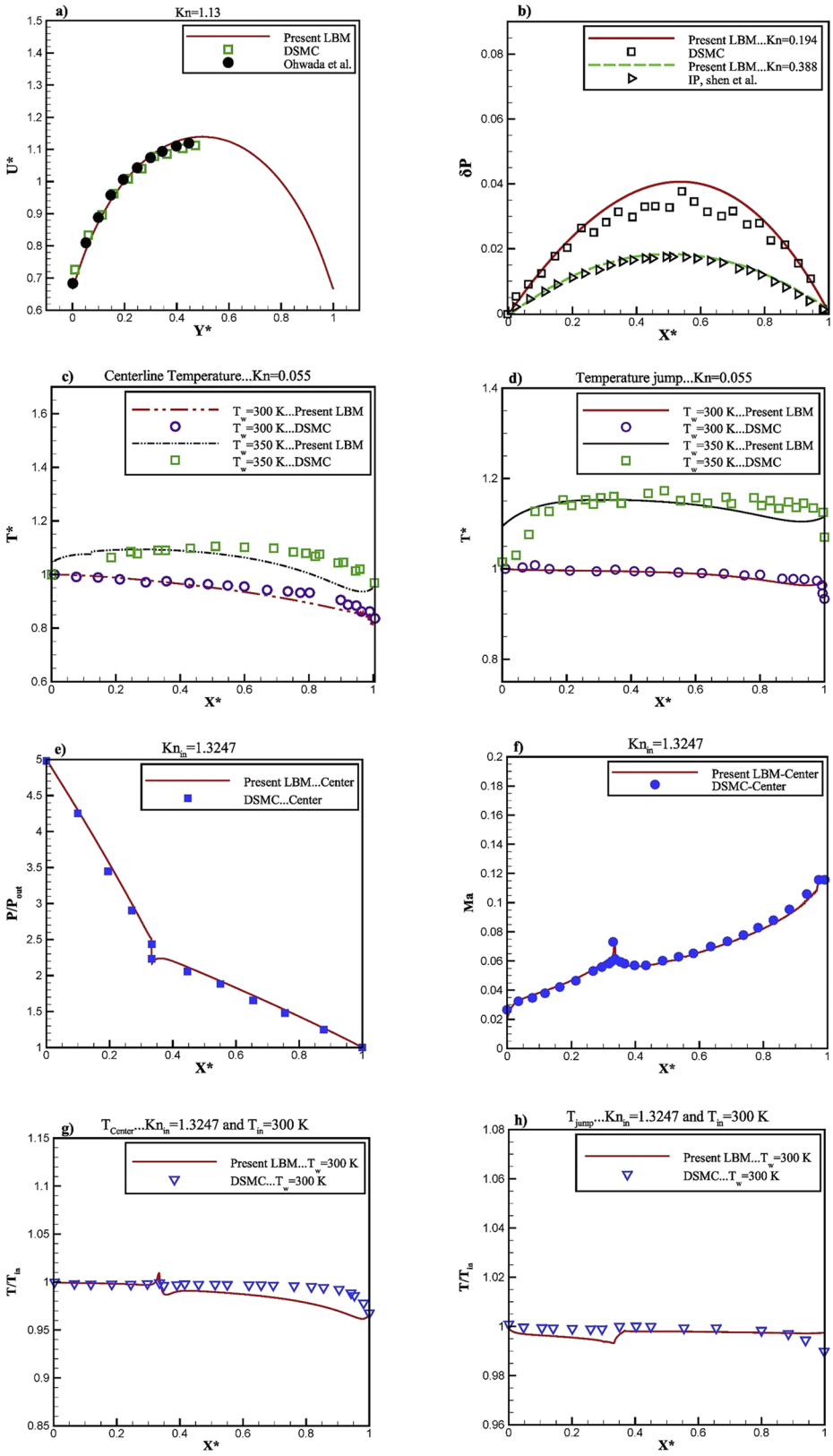

FIG. 2. Comparison between results of current LBM and other methods. (a) Non-dimensional velocity profile along the Y-direction at *Kn* = 1.13. (b) Pressure deviation from the linear pressure at outlet *Kn* numbers of 0.194 and 0.388. [(c) and (d)] Centerline temperatures and temperature jumps at Kn_{in} = 0.055 for wall temperatures of 300 K and 350 K. [(e)–(g)] The pressure, *Ma*, and temperature distribution along the centerline at *Kn* = 1.3247. (h) Temperature jump distribution at Kn_{in} = 1.3247.

TABLE II. Details of the chosen test case for thermal validation.

Case	Gas	$AR\ (L/H)$	Kn_{in}	M_{out}	P_{in} (kPa)	P_{out} (kPa)	PR	Heat condition (K)	Re_{in}	T_{in} (K)
1	*He*	4	0.055	0.586	108	308	2.851	$T_w = 300$	5.84	300
2	*He*	4	0.055	0.586	107	314	2.934	$T_w = 350$	5.20	300

TABLE III. Details of flow and heat conditions for the transition regime test case.

Gas	$AR\ (L/H)$	Kn_{in}	PR	ER	Heat condition (K)	Re_{in}	T_{in} (K)
Ar	10	1.3247	5	2	$T_w = 300$	0.052	300

velocity, and the pressure has a vice versa relationship with the velocity. In the microchannel with backward facing micro-step, change of the cross section has a crucial impact on the *Kn* number and pressure values such that the slope of the reducing pressure is decreased after the step due to the sudden increase in the channel cross section. Variations of the pressure will be better clarified in relation with the velocity distribution results shown in continue. Furthermore, the pressure is lower in the channel with the step due to the higher velocity as a result of lower flow area before the step.

Figures 4(a) and 4(b) show variations of the non-dimensional slippage velocity, slip velocity divided by the mean velocity, along the top wall for various inlet *Kn* numbers for microchannels with uniform and non-uniform cross sections, indicating that the slip velocity is increased with the *Kn* number. It is increased continuously along the straight microchannel as well because the *Kn* number is increased continuously along this channel. In Fig. 4(b), the slip velocity is reduced considerably after the micro-step due to the sudden area increase. The non-dimensional velocity profiles at various *Kn* numbers are also shown in Fig. 4(c) for the microchannel with uniform cross section. As observed, the slip velocity is increased with the *Kn* number, while the centerline velocity is decreased. The maximum velocity is at $Y^* = \frac{Y}{H} = 0.5$ and the shape of velocity profiles are parabolic. The streamwise velocity contour, expressed in lattice units, at the inlet $Kn = 1.1$ is shown in Figs. 4(d) and 44(e) for the uniform and with micro-step channels, respectively. As observed, the average and slip velocity are continuously increased in the uniform channel due to the decrease in the pressure and increase in the *Kn* number along the channel, respectively. For the channel with the micro-step, the same trend is observed, but with a discontinuity at the micro-step location in the form of a sudden decrease in the mean and slip velocities.

Figure 5 shows variations of the fluid mean Mach number ($Ma_{mean} = \frac{U_{mean}}{c_s}$) for three different inlet *Kn* numbers. For any *Kn* number in Fig. 5(a), the inlet *Ma* number is lower than the outlet one due to the $Kn_{out} = Kn_{in}$.Π relation and direct relationship between *Kn* and *Ma* numbers. Therefore, the mean velocity at the channel inlet is lower than that at the outlet. This incremental trend of the mean velocity along the uniform channel is in relation and in accordance with the pressure decrease along the channel shown before in Fig. 3(a). In other words, as mentioned earlier, the pressure and velocity trends are vice versa. The mean *Ma* number, or mean velocity, is sharply decreased at the location of the micro-step due to the sudden increase in the cross sectional area [Fig. 5(b)], as the mass flow rate is constant along the channel. This is why the pressure slope at the micro-step location is reduced in Fig. 3(b) because the mean velocity is decreased suddenly at this location, and there is a vice versa relationship between velocity and pressure. The mean Mach number increases with the decrease in the *Kn* number.

Variations in the non-dimensional velocity, $U^* = \frac{U}{U_{mean}}$, along the channels at $Y = H/2$ is also shown in Fig. 6, indicating that on the contrary of *Ma* variation in Figs. 5(a), U^* is decreased along

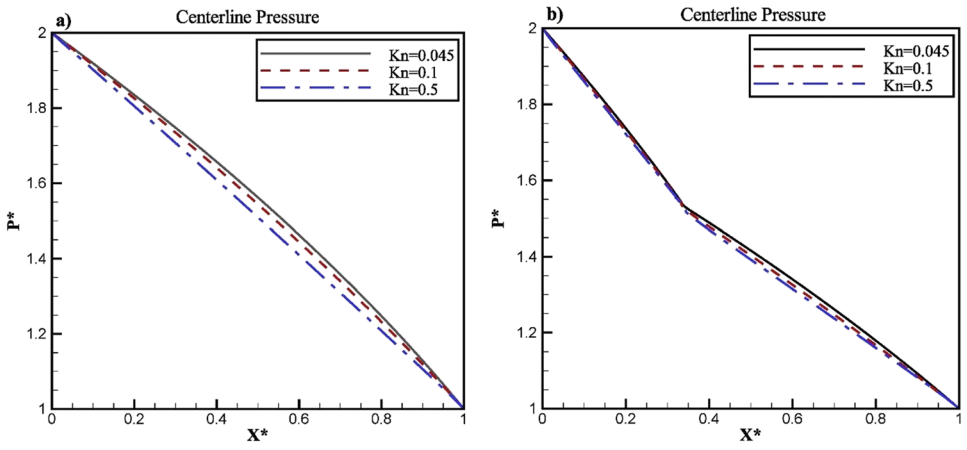

FIG. 3. Variation of the pressure along the channel at various inlet *Kn* numbers for a straight (a) and with-step (b) microchannels.

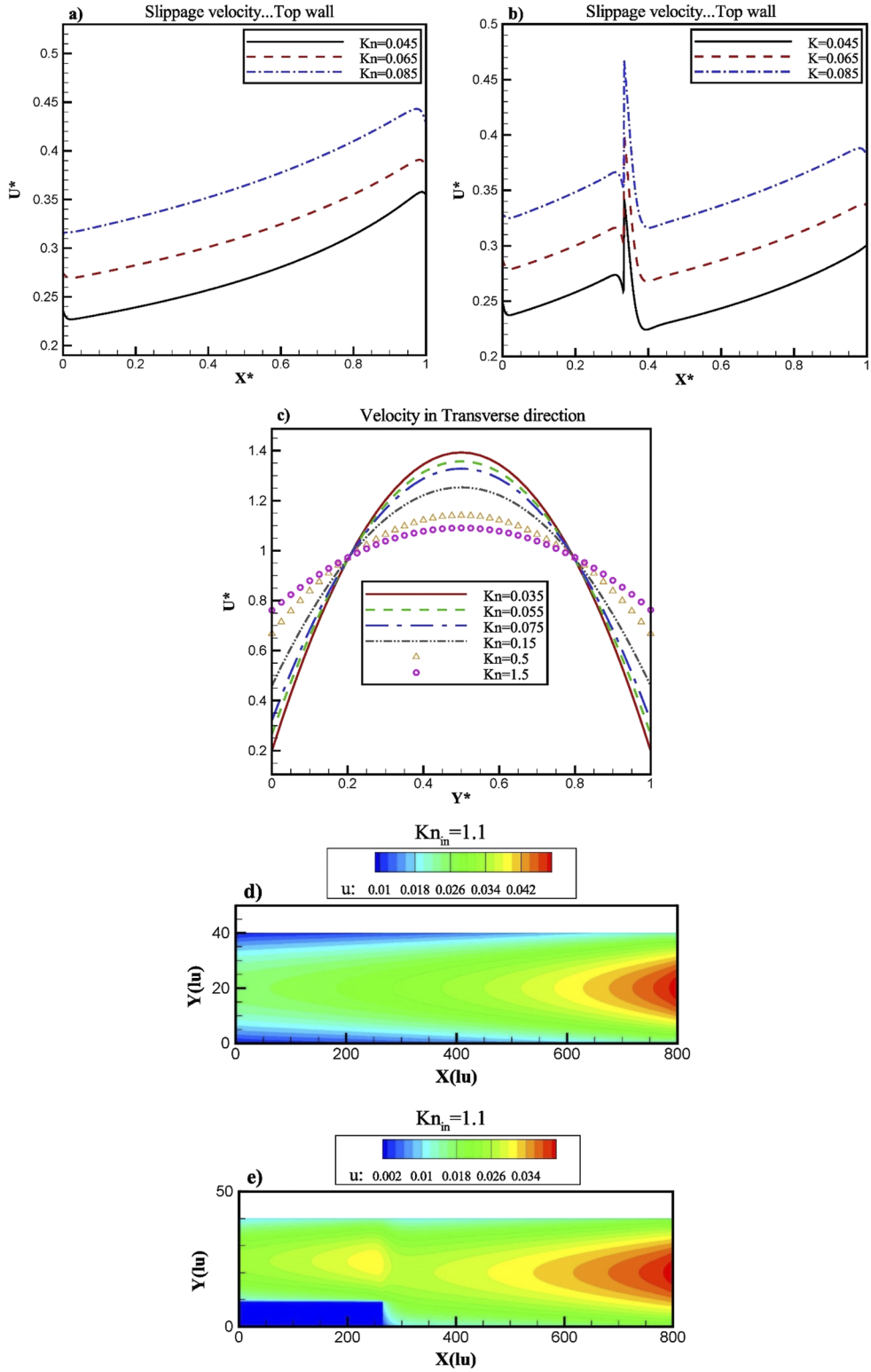

FIG. 4. Variations of the non-dimensional velocity slip on top wall; (a) no micro-step and (b) with a micro-step. (c) Velocity profile at various inlet *Kn* numbers in the uniform channel. [(d) and (e)] Streamwise lattice velocity contours at Kn_{in} = 1.1 for the uniform and with step channels.

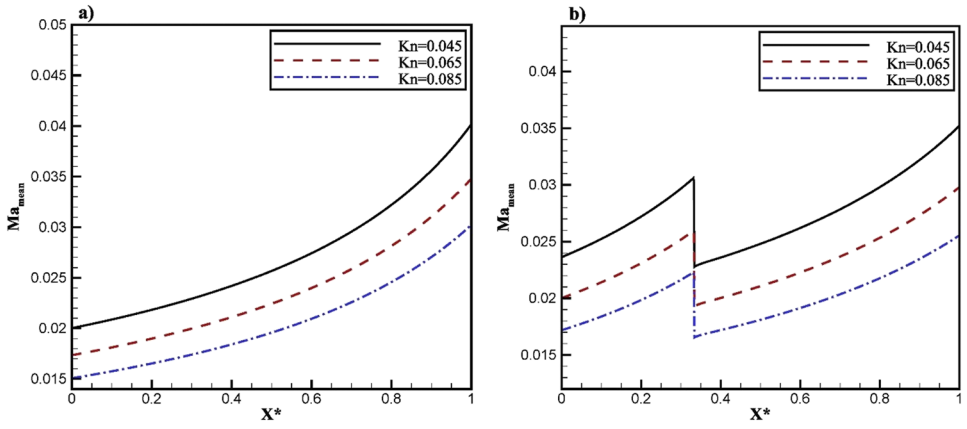

FIG. 5. Variations of the mean Mach number along the channel. (a) No micro-step and (b) with a micro-step.

the uniform microchannel because U_{mean} is increased along this microchannel. For the channel with the step, the average velocity is sharply decreased at the step [Fig. 5(b)], leading to a sharp increase at the step position observed in Fig. 6(b).

Figure 7 shows the streamlines near the micro-step at various *Kn* numbers. As observed, increasing the rarefaction suppresses the vortex due to a lower momentum and larger diffusion. Although the slippage is increased with the *Kn* number, re-enforcing the flow separation, the lower momentum and higher diffusion overcome the slippage increase.

For both regular and irregular shape microchannels, the variation in the non-dimensional temperature jump on the upper wall is depicted in Figs. 8(a) and 8(b), respectively. As observed, the temperature is sharply reduced in the narrow developing region and then reaches a constant value, which increases with the *Kn* number as expected. For the channel with the micro-step, the constant value is reduced slightly after the step and again becomes a constant. Figure 8(c) shows the dimensionless mean temperatures (relative to inlet temperature) along both the regular and irregular microchannels at three different Knudsen numbers. For any case, the nondimensional average temperatures decrease and there is an inverse relationship between *Kn* numbers and $T^*_{mean} = \frac{T_{mean}}{T_{in}}$.

The mean temperature is calculated by $T_{mean} = \frac{\int \rho u T dA}{\rho u_{mean} A}$, which is used to define the non-dimensional temperature as $T^* = \frac{T}{T_{mean}}$. Parameter A demonstrates the local area of geometry. Figures 9 (a) and 9(b) show variations of the non-dimensional temperature along the channel at $Y = H/2$ for channels with and without the micro-step at three inlet *Kn* numbers. The inlet temperature is set to $T_{in} = 1$ (Tu) and the wall temperature equals $T_w = 0$ (Tu) in lattice units. Therefore, T_{mean} is less than 1, which is decreased along the microchannel due to the cooling process. As observed in Figs. 9(a) and 9(b), the non-dimensional temperature increases with the increase in the *Kn* number. Furthermore, it is increased sharply in the small developing region and then increases very smoothly for the channel with no step. The entrance region is small mostly because the *Pr* and *Re* numbers are very low. For the micro-step channel, the temperature is increased sharply first, but the micro-step prevents the temperature to reach its highest value and regulates the upstream temperature to a moderate constant value. After the step, the non-dimensional temperature rises suddenly again due to the sudden velocity reduction and thus T_{mean} reduction, reaching an almost constant and the same maximum value as the no-step case. Figure 9(c) shows variations of the temperature profile at several sections along the uniform microchannel at the inlet *Kn* number of 0.035. As observed, the

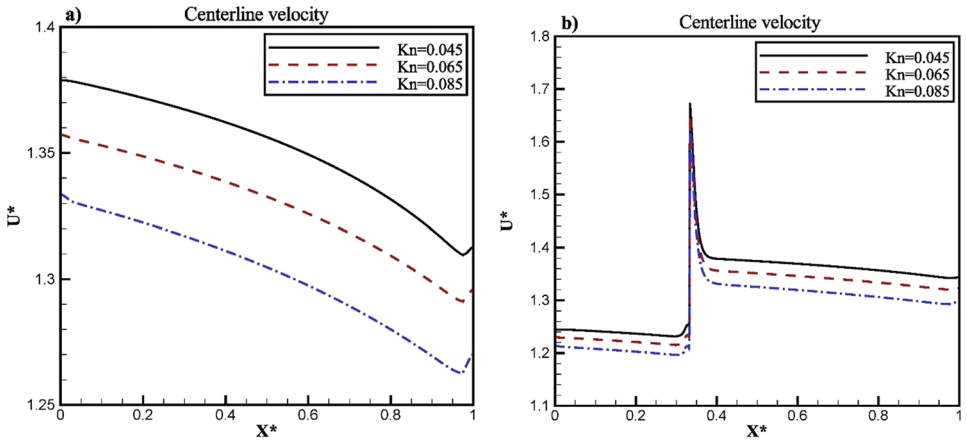

FIG. 6. Variations of the non-dimensional velocity along the channel centerline (Y* = 0.5). (a) No micro-step and (b) with a micro-step.

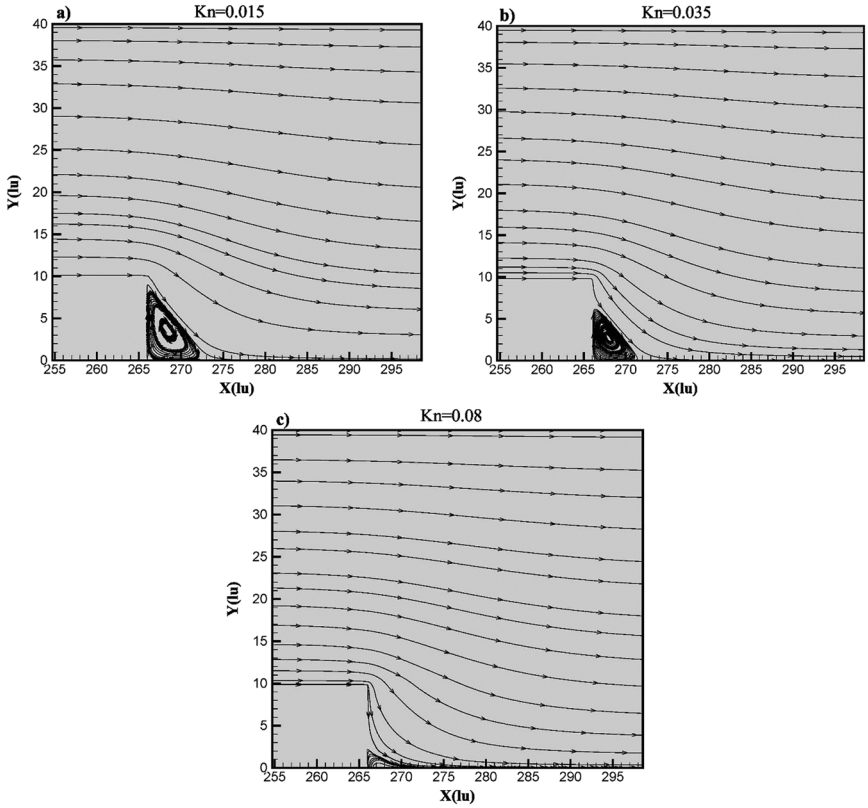

FIG. 7. Effect of the rarefaction on the flow separation and vortex generation at various Kn numbers. (a) Kn = 0.015, (b) Kn = 0.035, and (c) Kn = 0.08.

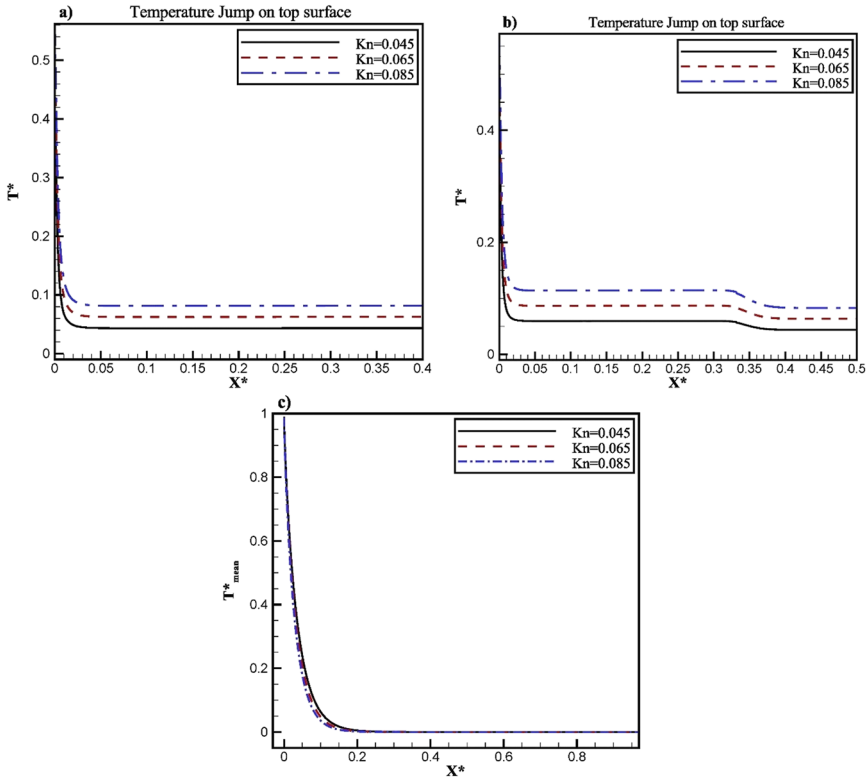

FIG. 8. Variations of the non-dimensional temperature jump on top wall at different inlet *Kn* numbers in the slip regime. (a) No micro-step, (b) with a micro-step, and (c) non-dimensional mean temperature distribution, the same distribution for both channels.

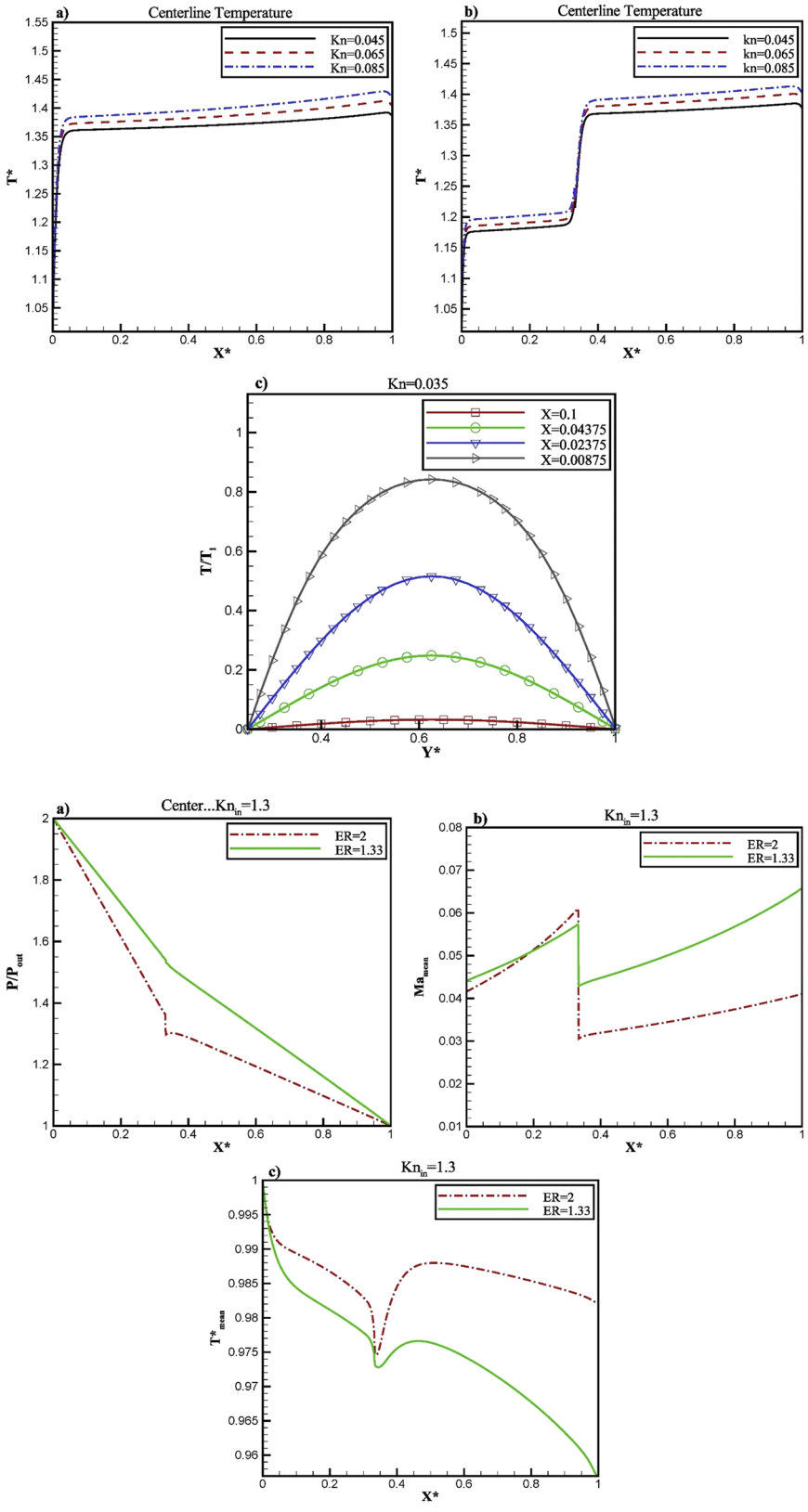

FIG. 9. Variations of the non-dimensional centerline temperature along the channel at different inlet *Kn* numbers in the slip regime. (a) Uniform cross section and (b) with a micro-step. (c) Temperature profile at various cross sections along the uniform channel.

FIG. 10. Effect of the expansion ratio of the channel with the micro-step on the (a) non-dimensional centerline pressure, (b) mean *Ma* number, and (c) mean temperature distributions along the channel. $T_i = T_w = 1(Tu)$, $PR = 2$, and $Kn_{in} = 1.3$.

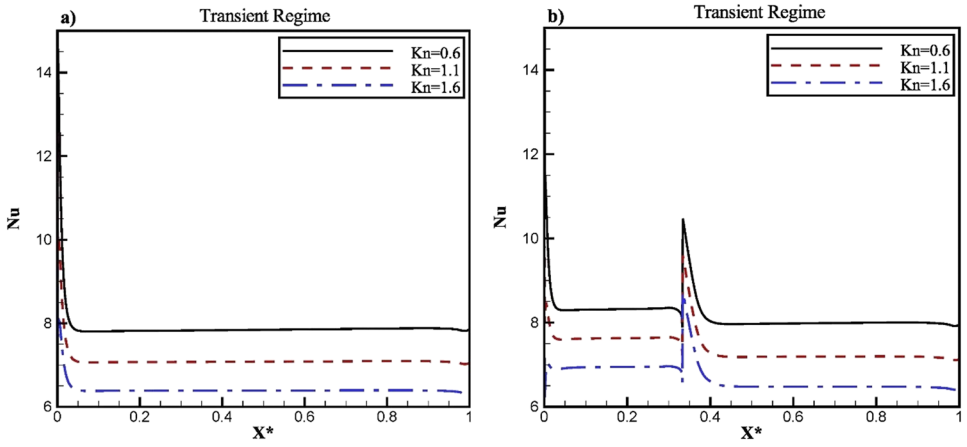

FIG. 11. Variation of the Nusselt number along the channel at different inlet *Kn* numbers in the transition regime. (a) No micro-step and (b) with a micro-step.

temperature gradient on the upper and lower walls reduces along the channel, indicating reduction of heat transfer. Furthermore, at $X^* = 0.1$, the fluid temperature almost reaches the wall temperature, $T_w = 0$ *Tu*.

Figure 10 shows effects of the micro-step height, characterized by the expansion ratio $ER = \frac{H_{out}}{H_{in}} = \frac{H}{H-h_s}$, on the pressure ($Y^* = 0.5$), *Ma* number, and mean temperature along the microchannel. The inlet and wall temperatures are set to 1 (*Tu*), $PR = 2$, and inlet $Kn = 1.3$. Figure 10(a) shows the pressure distribution, indicating that the pressure is lower for the channel with higher *ER*. This is justified by analyzing the relation between the *Kn*, *Ma*, and *Re* numbers, which is $Kn \propto \frac{Ma}{Re}$. This relation indicates that $Kn \propto \frac{1}{H-h_s}$; therefore, the *Kn* number is increased with the *ER* or the step height. Since the pressure is adversely proportional to the *Kn* number; therefore, the pressure is reduced with the *ER*. As observed in Fig. 10(b), the *Ma* number is reduced as the *ER* is increased because higher *ER* means lower inlet height of the channel and the flow rate and average velocity have direct relationship with the channel height. Therefore, for the same pressure gradient and channel length, the flow rate and velocity are reduced with the increase in the step height or the *ER*. Figure 10(c) shows distribution of the non-dimensional mean temperature, $T^*_{mean} = \frac{T_{mean}}{T_i}$, along the channel for two *ER* values. As observed, for both ER values, the temperature is reduced until the step location, where it is suddenly increased and then decreased again. The trend of the temperature is in relation with the velocity distribution shown in Fig. 10(b), indicating a vice versa relation between them. Furthermore, the mean temperature is slightly lower for the lower *ER* due to the higher mass flow rate.

Hadjiconstantinou and Simek[22] and Shokouhmand and Meghdadi Isfahani[38] reported the Nusselt number calculation as $Nu = \frac{2H\left(\frac{\partial T}{\partial y}\right)_w}{(T_w - T_{mean})}$. Using this relation, the *Nu* number is calculated and its variations along the channel at various inlet *Kn* numbers in the transition regime are shown in Fig. 11, indicating that the *Nu* number is reduced with the increase in *Kn* number due to the reduction of T_{mean} and $\left(\frac{\partial T}{\partial y}\right)$ on the top wall. Another analysis can be made considering $Nu = const. \times Re^{0.5}\, Pr^{0.33}$ reported by Bejan[39] for the flow in a coplanar channel; the constant equals 0.664 for the channel with constant cross section. Substituting *Re* from $Kn = \sqrt{\frac{\gamma\pi}{2}}\frac{Ma}{Re}$ and replacing $Ma = \frac{U}{c_s}$, the *Nu* number relation for the rarefied flow is obtained as follows:

$$Nu = const. \times \left(\sqrt{\frac{\gamma\pi}{2}}\frac{U}{c_s \cdot Kn}\right)^{0.5} \cdot Pr^{0.33}. \tag{19}$$

In Fig. 11(a), the Prandtl number, γ, and c_s are constant and the same, and the outlet *Kn* numbers are higher than 1 due to the $PR = 2$. For $Kn_{out} > 1$, the mass flow rate and mean flow velocity *U* are reduced with increase in the Kn_{out} number for the same *PR* and outlet pressure. Therefore, according to Eq. (19), $\frac{U}{Kn}$ is reduced and the *Nu* number is decreased as a result. Figure 11(b) indicates that the *Nu* number is increased by adding the micro-step due to the higher flow velocity as a result of lower flow area compared with the regular channel in Fig. 11(a). Furthermore, the *Nu* value after the step is reduced compared to the before-step value due to the velocity decrease as a result of area increase. Moreover, as observed in Fig. 11(b), the micro-step causes a sharp local increase in the *Nu* number.

V. CONCLUSION

A TRT-SRT LBM was implemented in this paper with the BSR velocity slip and second-order temperature jump boundary conditions to study the rarefied gaseous flow and heat transfer in a microchannel with a micro-step in slip and transition flow regimes. Results of the straight microchannel with no micro-step were also reported and compared with the with-step one to evaluate effects of the micro-step on the fluid flow and heat transfer for the same flow and heat transfer conditions. Main concluding remarks can be summarized as follows:

- By increasing the rarefaction, pressure values tend from non-linear to linear trend.
- The dimensionless velocity increases at micro-step length because of the cross section decrease, with sudden decreases just after the step as a result of the sudden cross section increase.

- Rarefaction affects the flow separation by changing the slippage and flow momentum.
- The fluid temperature and Nusselt number are sharply reduced in the narrow entrance region, and the diffusion time is very short compared to advection time.
- The non-dimensional temperature jump and centerline temperature are decreased and increased, respectively, after the micro-step and both increase with the Knudsen number.
- The Nusselt number is decreased with the increase in the Knudsen number for both channels. The step causes a positive pulse in the Nusselt number; however, after the step, the Nusselt number reaches the same value as in the case of the no-step channel.

DATA AVAILABILITY

The data that support the findings of this study are available from the corresponding author upon reasonable request.

REFERENCES

[1]Z. Guo, T. S. Zhao, and Y. Shi, "Physical symmetry, spatial accuracy, and relaxation time of the lattice Boltzmann equation for microgas flows," J. Appl. Phys. **99**, 074903 (2006).
[2]M. Shamseddine and I. Lakkis, "A novel spatio-temporally adaptive parallel three-dimensional DSMC solver for unsteady rarefied micro/nano gas flows," Comput. Fluids **186**, 1–14 (2019).
[3]R. Zakeri, R. Kamali-Moghadam, and M. Mani, "A new approach for chemical reaction simulation of rarefied gas flow by DSMC method," Comput. Fluids **140**, 111 (2016).
[4]H. Rostamzadeh, M. R. Salimi, and M. Taeibi-Rahni, "Pore-scale modeling of rarefied gas flow in fractal micro-porous media , using lattice Boltzmann method (LBM)," J. Therm. Anal. Calorim. **135**, 1931 (2018).
[5]J. Meng and Y. Zhang, "Accuracy analysis of high-order lattice Boltzmann models for rarefied gas flows," J. Comput. Phys. **230**, 835–849 (2011).
[6]M. Tuan, J. Li, L. Wu, J. M. Reese, and Y. Zhang, "A comparative study of the DSBGK and DVM methods for low-speed rarefied gas flows," Comput. Fluids **181**, 143–159 (2019).
[7]A. Taassob, R. Kamali, and A. Bordbar, "Investigation of rarefied gas flow through bended microchannels," Vacuum **151**, 197–204 (2018).
[8]A. Gavasane, A. Agrawal, and U. Bhandarkar, "Study of rarefied gas flows in backward facing micro-step using direct Simulation Monte Carlo," Vacuum **155**, 249–259 (2018).
[9]D. C. Guerrieri, A. Cervone, and E. Gill, "Analysis of nonisothermal rarefied gas flow in diverging microchannels for low-pressure microresistojets," J. Heat Transfer **138**, 1–11 (2017).
[10]M. Hadj-Nacer, D. Maharjan, M. Ho, S. K. Stefanov, I. Graur, and M. Greiner, "Continuum and kinetic simulations of heat transfer trough rarefied gas in annular and planar geometries in the slip regime," J. Heat Transfer **139**, 1–8 (2017).
[11]G. Biswas, M. Breuer, and F. Durst, "Backward-facing step flows for various expansion ratios at low and moderate Reynolds numbers," J. Fluids Eng. **126**, 362 (2004).
[12]V. A. Titarev, "Implicit high-order method for calculating rarefied gas flow in a planar microchannel," J. Comput. Phys. **231**, 109–134 (2012).
[13]M. Ho, J. G. Pérez, M. Reggio, and J. Trépanier, "Permeability calculation of rare filed gas flows through 2D porous structures using the lattice Boltzmann method," Phys. Chem. Earth **113**, 43 (2019).
[14]J. Wang, Q. Kang, Y. Wang, R. Pawar, and S. S. Rahman, "Simulation of gas flow in micro-porous media with the regularized lattice Boltzmann method," Fuel **205**, 232–246 (2017).
[15]S. Ansumali, "Hydrodynamics beyond Navier–Stokes : Exact solution to the lattice Boltzmann hierarchy," Phys. Rev. Lett. **98**, 124502 (2007).
[16]S. H. Kim, H. Pitsch, and I. D. Boyd, "Accuracy of higher-order lattice Boltzmann methods for microscale flows with finite Knudsen numbers," J. Comput. Phys. **227**, 8655–8671 (2008).
[17]L. M. Yang, C. Shu, J. Wu, and Y. Wang, "Comparative study of discrete velocity method and high-order lattice Boltzmann method for simulation of rarefied flows," Comput. Fluids **146**, 125–142 (2017).
[18]E. K. Ahangar, M. B. Ayani, and J. A. Esfahani, "Simulation of rarefied gas flow in a microchannel with backward facing step by two relaxation times using lattice Boltzmann method—Slip and transient flow regimes," Int. J. Mech. Sci. **157-158**, 802–815 (2019).
[19]S. F. Kharmiani and E. Roohi, "Rarefied transitional flow through diverging nano and microchannels: A TRT lattice Boltzmann study," Int. J. Mod. Phys. C **29**, 1850117 (2018).
[20]E. K. Ahangar, M. B. Ayani, J. A. Esfahani, and K. C. Kim, "Lattice Boltzmann simulation of diluted gas flow inside irregular shape microchannel by two relaxation times on the basis of wall function approach," Vacuum **173**, 109104 (2020).
[21]V. E. Ambrus and V. Sofonea, "Lattice Boltzmann models based on half-range Gauss–Hermite quadratures," J. Comput. Phys. **316**, 760–788 (2016).
[22]N. G. Hadjiconstantinou and O. Simek, "Constant-wall-temperature Nusselt number in micro and nano-channels," J. Heat Transfer **124**, 356 (2002).
[23]M. Renksizbulut, H. Niazmand, and G. Tercan, "Slip-flow and heat transfer in rectangular microchannels with constant wall temperature," Int. J. Therm. Sci. **45**, 870–881 (2006).
[24]O. I. Rovenskaya, "Computational study of 3D rarefied gas flow in microchannel with 90 bend," Eur. J. Mech. B/Fluids **59**, 7–17 (2016).
[25]X. D. Niu, C. Shu, and Y. T. Chew, "A thermal lattice Boltzmann model with diffuse scattering boundary condition for micro thermal flows," Comput. Fluids **36**, 273–281 (2007).
[26]Z.-W. Tian, C. Zou, H.-J. Liu, Z.-L. Guo, Z.-H. Liu, and C.-G. Zheng, "Lattice Boltzmann scheme for simulating thermal micro-flow," Physica A **385**, 59–68 (2007).
[27]S. Gokaltun and G. S. Dulikravich, "Lattice Boltzmann method for rarefied channel flows with heat transfer," Heat Mass Transfer **78**, 796–804 (2014).
[28]H. F. Tan, J. T. Kang, and C. G. Wang, "Study on grooved wall flow under rarefied condition using the lattice Boltzmann method," Int. J. Mech. Sci. **90**, 1–5 (2015).
[29]J. Wang, L. Chen, Q. Kang, and S. S. Rahman, "The lattice Boltzmann method for isothermal micro-gaseous flow and its application in shale gas flow: A review," Int. J. Heat Mass Transfer **95**, 94–108 (2016).
[30]A. A. Mohamad, *Lattice Boltzmann Method* (Springer-Verlag London Limited, 2011).
[31]A. Homayoon, A. H. M. Isfahani, E. Shirani, and M. Ashrafizadeh, "A novel modified lattice Boltzmann method for simulation of gas flows in wide range of Knudsen number," Int. Commun. Heat Mass Transfer **38**, 827–832 (2011).
[32]S. K. Loyalka, "Approximate method in the kinetic theory," Phys. Fluids **14**, 2291–2294 (1971).
[33]Q. Li, Y. L. He, G. H. Tang, and W. Q. Tao, "Lattice Boltzmann modeling of microchannel flows in the transition flow regime," Microfluid. Nanofluid. **10**, 607–618 (2011).
[34]E. Roohi and M. Darbandi, "Extending the Navier–Stokes solutions to transition regime in two-dimensional micro- and nanochannel flows using information preservation scheme," Phys. Fluids **21**, 082001 (2009).
[35]T. Ohwada, Y. Sone, and K. Aoki, "Numerical analysis of the Poiseuille and thermal transpiration flows between two parallel plates on the basis of the Boltzmann equation for hard-sphere molecules," Phys. Fluids A **1**, 2042–2049 (1989).
[36]C. Shen, J. Fan, and C. Xie, "Statistical simulation of rarefied gas flows in microchannels," J. Comput. Phys. **189**, 512–526 (2003).
[37]E. Roohi, M. Darbandi, and V. Mirjalili, "Direct simulation Monte Carlo solution of subsonic flow through micro/nanoscale channels," J. Heat Transfer **131**, 1–8 (2009).
[38]H. Shokouhmand and A. H. Meghdadi Isfahani, "An improved thermal lattice Boltzmann model for rarefied gas flows in wide range of Knudsen number," Int. Commun. Heat Mass Transfer **38**(10), 1463–1469 (2011).
[39]A. Bejan, *Convection Heat Transfer* (John Wiley & Sons, Inc., New Jersey, 2013).